Tilting and transpression of an Archaean anorthosite in northern Ontario

Graham J. Borradaile, France Lagroix, David King

ELSEVIER

Tectonophysics 293 (1998) 239–254

TECTONOPHYSICS

Tilting and transpression of an Archaean anorthosite in northern Ontario

Graham J. Borradaile *, France Lagroix, David King

Geology Department, Lakehead University, Thunder Bay, ON P7B 5E1, Canada

Received 11 September 1997; accepted 12 March 1998

Abstract

An Archaean anorthosite complex crops out over more than 300 km^2 at the junction between an Archaean metasedimentary accretionary prism (Quetico Belt) and a volcanic greenstone terrain to the north (Wabigoon Belt). The anorthosite is feebly deformed and weakly foliated. However, anisotropies of low field susceptibility (AMS) and anhysteretic remanence (AARM) define consistent magnetic fabric directions extending over subareas >25 km^2 in extent. Whereas magnetic fabrics cannot define strain magnitudes, they normally provide reliable indications of finite strain orientations, even where the fabrics developed by stress-controlled nucleation during a progressive noncoaxial strain history. The field schistosity S_1, being the oldest foliation, rotated closest to the shear plane. AMS foliation due to preferred crystallographic orientation of silicates and pyrrhotite as well as preferred dimensional orientation of magnetite lies at a greater angle to the shear plane; because it formed late then S_1 had less time to rotate. The few measurements of the youngest AARM foliation caused by magnetite and pyrrhotite suggest that it may lie at a still greater angle to the shear plane. Thus, S_1 and succeeding magnetic foliations provide a cryptic shear-sense indicator. They reveal relative motions along the terrain boundary that include transpression due to NW–SE shortening causing dextral E–W shear with a north-side-up component. Palaeomagnetic data confirm a progressive northwards steepening of the anorthosite sills that is consistent with northwards subduction of the accretionary prism to the south.

Keywords: magnetic fabrics; kinematics; Archean terrains; rock magnetism; magneto-tectonics

1. Introduction

The Rainy Lake area lies in the Superior Province of the Canadian Shield, where the Archaean country rocks cooled from their ultimate metamorphic pulse ~2.7 Ga ago (Percival, 1989). The Province is separated into alternating EW subprovinces of greenstone–granitoid terrain and metasedimentary terrain with the fault-bounded Rainy Lake block situated between the Wabigoon Greenstone terrain to the north and the Quetico metasedimentary terrain to the south (Fig. 1). Much of the regional geology can be learned from Hudleston (1976), Sawyer (1983), Hudleston et al. (1988), Williams et al. (1992), Bauer et al. (1992).

Two almost east–west, dextral, transcurrent faults bound the Rainy Lake block that hosts a gabbroic–anorthositic complex (Fig. 1). The anorthosites comprise three sheets, the thickest being about 6 km at its widest and at least 40 km along strike. General geological considerations and aeromagnetic interpre-

* Corresponding author. Tel.: +1 (807) 935-2753; Fax: +1 (807) 935-2753; E-mail: borradaile@lakeheadu.ca

0040-1951/98/$19.00
PII S0040-1951(98)00077-8

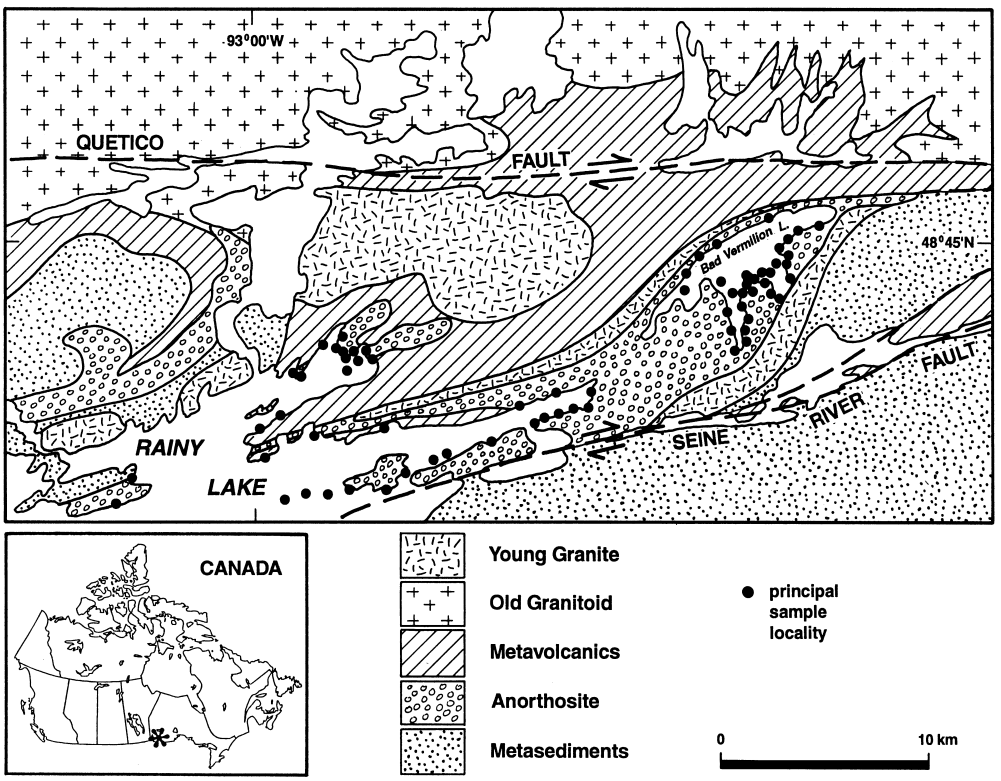

Fig. 1. Location of the area studied. The region north of the Quetico Fault is the Wabigoon granite–greenstone terrain, and the Quetico metasedimentary terrain lies south of the Seine River Fault.

tation (Fig. 2) show that the bodies dip steeply, as tilted sills, approximately parallel to the steep-bedded volcanic rocks in the north and the metasedimentary rocks to the south. However, the bedded sequences are isoclinally folded at least on scales of several outcrops. Thus, we are not dealing with a simple stratified sequence of sedimentary and volcanic rocks although the anorthosite sills remained rigid, subject only to minor flexure and acquired very weak, cataclastic fabrics.

The absence of good strain markers in the region encourages the use of magnetic fabrics to evaluate the shear sense and principal fabric directions (lineation and foliation). In adjacent areas one observes dextral transpression of the margins of the Quetico Belt (Borradaile et al., 1993a; Borradaile and Dehls, 1993) and north-side-up shear of the metasedimentary terrain immediately to the north of the Wabigoon Belt (Borradaile et al., 1993b). Elsewhere in the region, the orientation distribution of rock-forming silicates mainly influences the principal susceptibility directions in the metamorphic rocks. Physical separations of minerals or leaching tests (Borradaile et al., 1990) and hysteresis studies can distinguish, to various degrees, the paramagnetic and 'ferromagnetic' contributions to bulk susceptibility (Borradaile and Werner, 1994). The general conclusion is that AMS principal directions define a foliation due to an orientation distribution of mineral grains initially aligned by stress-controlled nucleation and subsequently modified by strain (Henry, 1990; Werner and Borradaile, 1996; Borradaile and Henry, 1997).

Anisotropy of anhysteretic remanence (AARM) extends the analysis by isolating the preferred mineral orientations of the 'ferro'-magnetic grains (Jackson, 1991; McCabe et al., 1985; Jackson and Tauxe, 1991). Where the ferromagnetic response is primarily due to magnetite grains, the AMS response reveals their *shape*-fabric or preferred dimen-

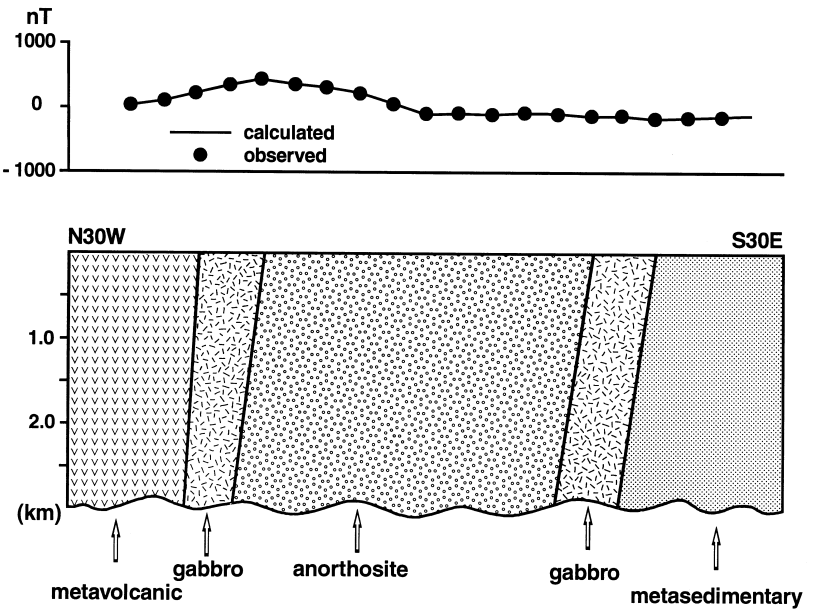

Fig. 2. Interpretation of the aeromagnetic anomalies using known susceptibility values for the rocks yields the above solution for the structures at depth. Note the vertical or steep, northwards dipping structures. The line of the section is through the centre of the Rainy Lake anorthosite.

sional orientation, due to the high susceptibility, low anisotropy and the demagnetizing effect.

On the other hand, AMS combines responses from paramagnetic (mafic) silicates and ferromagnetic grains, with a normally negligible, diamagnetic contribution from quartz, feldspar, etc. Where the ferromagnetic response is minor, the AMS signal largely shows the preferred crystallographic orientation of the mafic silicates (Borradaile and Henry, 1997). If the ferromagnetic response forms a significant portion of the signal, say $>5\%$, isolating the ferromagnetic and paramagnetic contributions is advisable (Jackson, 1991; Rochette et al., 1992; Borradaile and Werner, 1994). This may then be subtracted from the AMS response to determine the paramagnetic AMS fabric. In this way the silicate matrix fabric (paramagnetic) and accessory (ferromagnetic) fabrics are separated.

Thus, AMS may identify subtle variations in planar (S-tectonite) or linear (L-tectonite) silicate preferred crystallographic orientations whereas AARM determines the preferred orientation of higher susceptibility ferromagnetic grains. For magnetite this would be a preferred *dimensional* orientation. Of course, the strengths of these orientation distributions do not directly correlate with strain magnitudes or principal stress ratios, primarily because different proportions of minerals change the bulk anisotropy more than variation in preferred orientation (Borradaile, 1987a). Nevertheless, the principal directions of the AMS tensor normally faithfully represent strain directions that are near the finite state axes $X \geq Y \geq Z$ (Borradaile, 1988, 1991; Borradaile and Henry, 1997). AMS fabrics thus reveal an ellipsoid most often influenced by the orientation distribution of silicate-matrix minerals.

In this study, magnetic fabrics are particularly useful because the anorthosite complex provides only exceptionally coarse-grained rocks of low ductility with low contents of phyllosilicates. Thus, schistosity is rough, poorly developed and difficult to measure. It is largely a spaced cleavage of a cataclastic character (Borradaile et al., 1982). Field lineations are still more difficult to discern. Thus, observing L–S fabric variations in the field is not possible as in most other tectonically deformed rocks in the region.

Paramagnetic mafic silicates such as chlorite, biotite, amphibole and epidote have intrinsic bulk susceptibility <2000 μSI. Where susceptibilities are

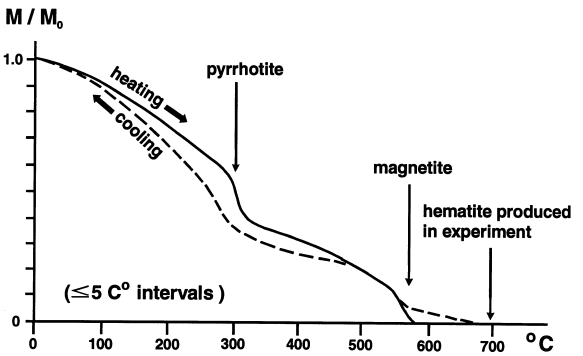

Fig. 3. Curie points determined from a Sapphire Instruments translation balance reveal that pyrrhotite and magnetite are present in most samples. Traces of hematite may be present initially in some samples but generally this is an artefact of the experiment.

higher, this may be due to inclusions of iron oxides or sulfides (Borradaile and Werner, 1994; Borradaile, 1994). Thus, even if the rocks were composed entirely of such silicates, their bulk susceptibility would be $\leq$2000 μSI. However, the mean bulk susceptibility of 276 samples is 6058 μSI. This shows that high susceptibility iron oxides or sulfides occur as traces. Thus, these grains dominate the AMS signal that combines of ferromagnetic, paramagnetic and diamagnetic contributions.

Thermomagnetic tests in a Sapphire Instruments translational Curie balance on concentrated mineral separations show that the remanence-bearing, high susceptibility phases are pyrrhotite and magnetite (Fig. 3). Moreover, it was subsequently found that the bulk anhysteretic remanence of 39 suitable samples was 164 mA/m; thus, the samples have the potential to carry a substantial remanence.

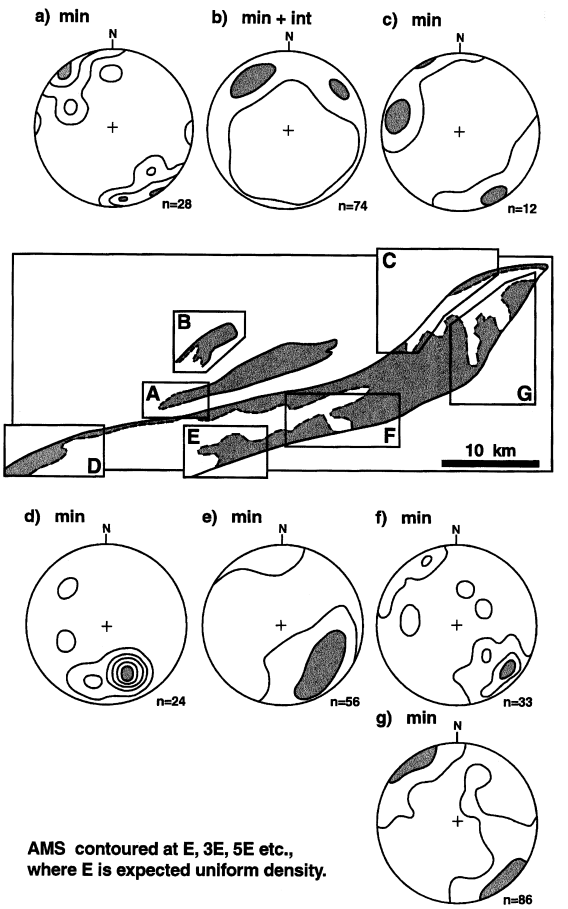

Fig. 4. Orientations of minimum susceptibility (and intermediate where the magnetic fabric is constricted, L>S) for the anorthosites in seven subareas. Throughout the anorthosites a magnetic foliation trending NE–SW is discernible, to which the pole concentration of minima is orthogonal. The exception is subarea B where fabrics are constricted causing a horizontal girdle of minimum susceptibility axes, defining a vertical magnetic fabric lineation.

2. Anisotropy of magnetic susceptibility (AMS)

We sampled 276 cores, of standard 1 inch diameter and 0.85 inches in height. At least two cores were taken from each oriented hand sample. The main sampling subareas are A through G, shown in the inset maps of Figs. 4 and 5.

Anisotropy was measured using the seven-orientation scheme of Borradaile and Stupavsky (1995) with a Sapphire Instruments SI2B unit at 19,200 Hz with an RMS field of 0.7 oersted. Sensitivity is 2×10^{-8} SI under good operating conditions. This provides ample resolution for the lowest susceptibility samples ($\sim$50 μSI) provided the body diagonal measurements are included and the appropriate checks for fabric homogeneity are applied for low susceptibility samples (Borradaile and Stupavsky, 1995). Most orientation distributions show a point concentration of minimum AMS axes defining a NE–SW foliation (S-fabric) that dips steeply north through most of the anorthosite (Fig. 4A, C, D, E, F, G). Subarea B differs in having a partial girdle of

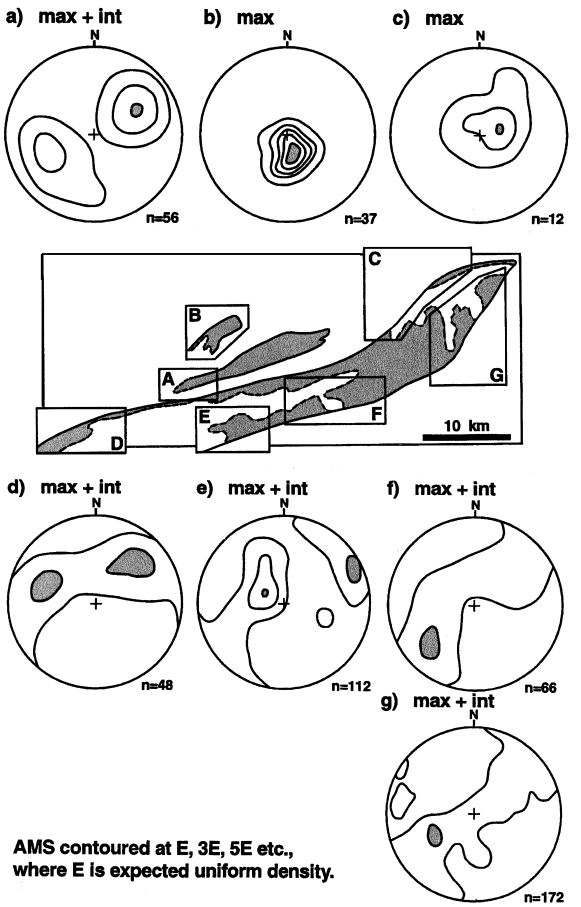

Fig. 5. Maximum susceptibility axial directions are shown for the anorthosite, with intermediate axes where the subareas A, D, E, F, G have flat-shaped magnetic fabric ellipsoids (S > L). Thus, in those five subareas, the maximum and intermediate axes define a crude girdle defining the magnetic fabric foliation. In subareas B and C linear fabrics dominate with nearly vertical magnetic lineations.

minimum axes, due to a more constricted fabric with a steep lineation.

The maximum axes combine the zone axis of long axes of paramagnetic silicates, the preferred dimensional orientation of magnetite and preferred crystallographic orientation of pyrrhotite. This is a composite magnetic lineation. Most fabrics tend to be oblate (S>L tectonites). Therefore combining maximum and intermediate axes in most subareas is more meaningful (Fig. 5). NE–SW foliations are apparent from the girdles of maximum and intermediate susceptibilities in all subareas, except in the north (Fig. 5B, C). In the latter, L>S fabrics suggest constriction about a steep axis.

3. Anisotropy of anhysteretic remanent magnetization (AARM)

We determined remanence anisotropy for 39 samples to isolate the fabric contribution of the remanence-bearing grains. Remanence was applied in seven directions, including the body diagonals of the samples (Borradaile and Stupavsky, 1995) to provide a rapid and precise estimate of anisotropy (Werner, 1997). Experiments show that this procedure does not require AF demagnetization between each stage of application of ARM (Werner and Borradaile, 1996). The principal directions of AARM are shown in Fig. 6. AARM was applied in a Sapphire Instruments AF demagnetizer from a peak field of 150 mT with a constant DC bias field of 1 oersted over a window from 100 mT to zero.

Most samples reveal only slight angular differences between the principal AMS and AARM axes. However, they are consistent in a way that may be attributed to fabric development during noncoaxial tectonic strain increments (Borradaile and Henry, 1997). We did not find ‘inverse’ fabrics, in which AMS axes do not correspond to AARM axes due to the presence of some single-domain magnetite or other mineral whose long axis coincides with minimum susceptibility (Stephenson et al., 1986; Rochette et al., 1992). The ferromagnetic accessories are large intercrystalline, multidomainal or large pseudo-single-domain grains scattered through the matrix. Little remanence is carried by the sparse inclusions in the feldspars (see Borradaile, 1994; Borradaile and Werner, 1994).

4. Comparison of AMS and AARM magnetic fabrics

The shape of magnetic fabric ellipsoids may correspond generally with the symmetry and eccentricity of the causative mechanism (Borradaile, 1988; Henry, 1989, 1990; Housen and van der Pluijm, 1990; Borradaile and Henry, 1997). For example, a constrictive strain event will produce an orientation

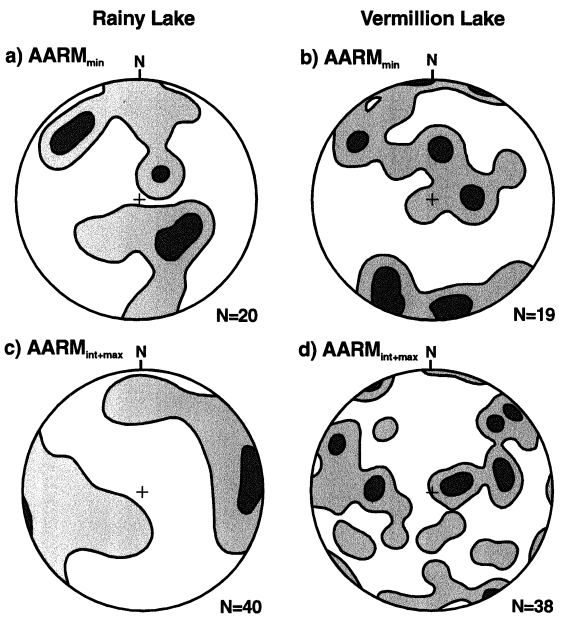

Fig. 6. Anisotropy of remanence isolates the contribution of ferromagnetic minerals, whereas low field susceptibility (Figs. 4 and 5) combines contributions from all minerals. Here remanence anisotropy was determined using anhysteretic remanence in a Sapphire Instruments AF demagnetizer. AARM is less well defined than AMS (Figs. 4 and 5) because fewer samples are suitable for AARM analysis. Moreover, the fabrics are controlled by smaller grain populations in each sample that causes a significant inter-sample scatter. Rainy Lake samples (a, c) show a poorly defined foliation ENE–WSW with a subhorizontal fabric lineation that would represent average maximum grain dimensions. Near Vermillion Lake the fabrics are less homogeneous (b, d).

distribution of minerals whose long axes define a marked lineation without foliation. The constrictive strain would be represented in symmetry alone by a rod-shaped magnetic fabric ellipsoid. In a coaxial strain history, the AMS (older silicates) and AARM (younger ferromagnetic) fabric ellipsoids may have a similar shape and their foliations would be parallel. However, each mineral has a different magnetic anisotropy and the AMS signal combines all their responses. Thus, at best, AMS can yield only a general impression of the crystals' orientation distribution. Moreover, in our case, the same can be said of AARM because it combines the response of magnetite and pyrrhotite preferred orientations. Moreover, the shapes of magnetic and fabric ellipsoids must always differ if they depart from perfectly prolate or oblate symmetry, even for a coaxial strain history.

The eccentricity of the fabric ellipsoid represents the intensity of the magnetic fabric and the crystallographic or grain orientation distribution that causes it. Unfortunately, this fabric parameter does not relate directly to finite strain magnitudes nor stress differences during recrystallization because the intrinsic anisotropy of the minerals overrides the anisotropy of the causative mechanism, e.g., finite strain or magmatic flow (Borradaile, 1988, 1991). As an extreme example a saturation alignment of mica can arise readily through stress-controlled nucleation. This would not represent the perfect alignment produced by infinite strain of initially dispersed micas.

$T_j = +1$ represents a perfect disk-fabric and $T_j = -1$ describes a perfect rod-fabric (Jelinek, 1981). P_j describes the eccentricity or intensity of fabric, for a sphere $P_j = 1$. The AMS ellipsoids of 276 samples define clearly a concentration in the field of flattened fabrics close to the origin (Fig. 7,

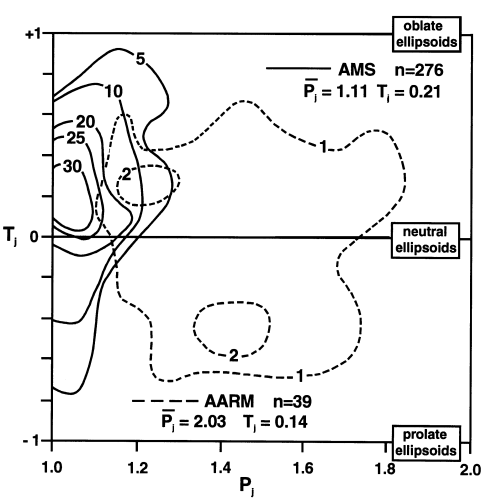

Fig. 7. Jelinek (1981) plot of the AMS and AARM fabric ellipsoid shapes. The frequency of points is given in counts per percentage area of the graph. Note that AMS fabrics are dominantly flat-shaped, due to the influence of the intrinsic anisotropy of phyllosilicate lattices. However, the data also cluster more closely to the neutral shape ($T_j = 0.21$) than for most phyllosilicates. This is due to the combined contributions from remanence-bearing grains. Their anisotropy was isolated by studying anhysteretic remanence (dashed contours) that show much higher anisotropy ($P_j > 1.2$ mostly) but more neutral shape on average ($T_j = 0.14$). Average P_j and T_j values are given on figure.

Table 1
Magnetic fabric parameters

	No. of samples	Mean bulk	P_j	T_j	X	Y	Z
AMS	276	6058 μSI	1.11	0.21	1.04	1.01	0.95
AARM	39	164 mA/m	2.03	0.14	1.27	1.07	0.78

Table 1). Thus, they suffered mild flattening due to an S>L orientation distribution of crystals and grains. Although paramagnetic silicates form a significant part of the AMS fabric, AARM isolated the contribution due to pyrrhotite and magnetite. AARM shows higher anisotropy intensity (P_j, Fig. 7, Table 1) than for AMS in which mafic silicates play an important role. Of course, this does not mean that the magnetite and pyrrhotite are strained more than the mafic silicates; their lattices are just more anisotropic. In fact, the magnetite and pyrrhotite formed later in the metamorphic sequence from textural evidence and general metamorphic considerations. Thus, they strained and rotated less than the silicate matrix. Differences between symmetry of the remanence-bearing grains (solely AARM) and silicates (included in AMS) are clear. AARM fabric ellipsoids for magnetite are normally more neutral ($\Rightarrow$0) than those of the accompanying AMS fabric. Again, this reflects a difference in crystallographic magnetic properties rather than a tectonic process. It is even possible that the symmetry (T_j) of the causative mechanism, e.g., syncrystallization differential or finite strain, was identical during formation of the remanence-bearing grains and the silicates. This tentative statement relies on the fact that crystallographic influence on magnetic anisotropy is normally more effective than deformation mechanisms.

In summary, AMS foliation planes for the seven subareas are shown in Fig. 8 with the mean AARM foliations for the two larger areas of Bad Vermillion and Rainy Lake. The range of angles between the AMS foliations in different subareas shows the fabric is regionally heterogeneous. By inference the controlling mechanisms, e.g., syncrystallization stress or strain, were similarly heterogeneous in orientation and intensity. Foliation planes vary over a range of slightly more than 45°. Significantly, AARM foliation planes are significantly discordant with the AMS foliation planes in the same subareas. Petrographic evidence and general metamorphic consideration shows that the accessory magnetite and pyrrhotite formed late. Remanence studies and Curie balance data (Fig. 3) show they are responsible for the AARM.

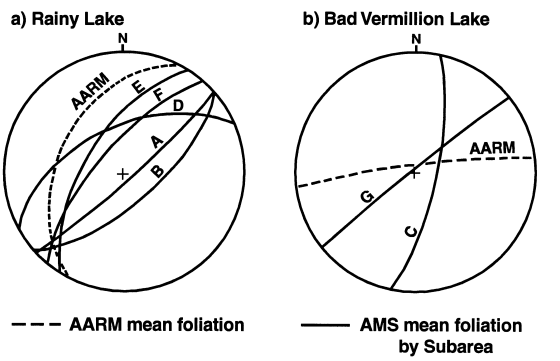

Fig. 8. Mean magnetic foliation planes for the main part of the Anorthosite intrusion near Rainy Lake (a) and the part sheared and deflected near Bad Vermillion Lake (b). *A* through *G* refer to the subareas of Figs. 4 and 5.

When a planar fabric is locked into a rock, whether by pressure solution, preferred nucleation orientation of neocrysts or one of many other deformation mechanisms, it becomes a strain marker. Generally, it is indelible in the absence of a complete metamorphic overprint so that it will spin during a subsequent noncoaxial strain history. We shall assume homogeneous strain, i.e., straight lines will remain straight and parallel lines remain parallel. The planar marker may be considered passive (i.e., of exactly the same ductility as the matrix) or to have different properties in which case particle–matrix viscosity contrast influences spin rate.

For the passive plane, and sometimes for the active plane, the spin rate exceeds the apparent rotation of the strain ellipsoid (Fig. 9). For perfect simple shear, with the necessary constraints on vorticity with incremental extensions applied at 45° to the shear plane, and no strain in the *Y*-direction, the strain ellipse and any planar marker rotates in-

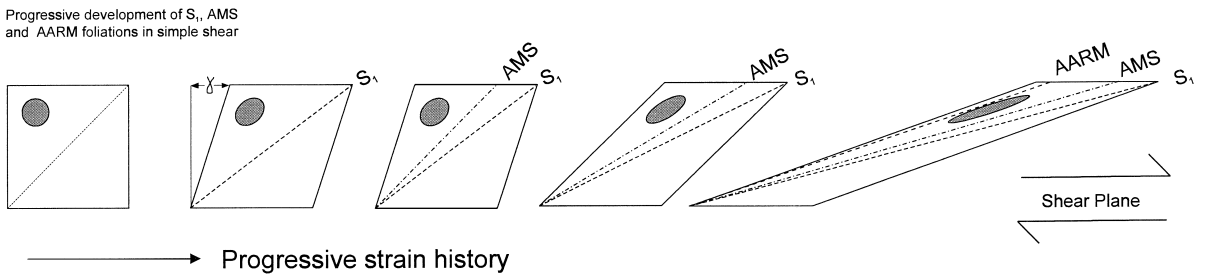

Fig. 9. Model of progressive development of foliations in perfect simple shear assuming homogeneous strain. On the extreme left, the initial fabric S_1, is initiated at 45° to the shear plane. With a shear strain γ it spins toward the shear plane. Then, an AMS foliation is initiated, again at 45° to the shear plane. Both fabrics subsequently rotate further toward the shear plane. Finally and AARM foliation develops and all three foliations continue to spin toward the shear plane.

definitely, but at different rates toward the shear plane until they become parallel at infinite strain. This 'progressive' strain is most common. However, under certain circumstances of vorticity the strain ellipse may pulsate, returning periodically to a sphere during the strain history (Ramberg, 1975). Such situations are unlikely to be relevant in magnetic fabric studies where the upper limit on magnetic anisotropy is dictated crystallographically. Moreover, for the large shear strains associated with pulsating histories (e.g., mylonite zones) deformation mechanisms may completely reset the magnetic anisotropy periodically. Thus, in rare pulsating strain histories, magnetic fabric will at best only record a fraction of the strain history, perhaps less than one half-cycle of pulsation.

When multiple planar *XY* marker develop asynchronously during progressive strain their relative angles should reveal the shear sense, by analogy with S–C fabrics of classical structural geology. The oldest anisotropy plane (S_1 cataclastic field foliation) should always lie most nearly parallel to the shear plane (Fig. 9). Successively younger foliations such as AMS influenced by mafic silicate fabric and AARM due to the ferromagnetic fabric lie at greater angular distances from the shear plane since they are initiated at 45° to the shear plane in simple shear at some later stage in the strain history. Of course, for very large shear strains (γ, Fig. 9) this may be invalid because the different rheologies of the minerals defining each subfabric might rotate at different relative rates to those assumed in Fig. 9, causing different relative angular relations. This is not possible in this region because the strain is so low, and it would be unlikely in most other metamorphic rocks. S_1 was established by minor strain of the feldspars in the anorthosite, whereas AMS and AARM were frozen into the rocks by stress-controlled preferred orientation crystallization and then strained. With the low strains in our region (much less than in Fig. 9) the relative angular relations confirm consistent shear sense. Under these circumstances, the initial AMS and AARM foliations should be nearly parallel to the principal *XY* plane of the appropriate strain ellipsoid *at the time of formation* of each magnetic subfabric. Relative orientations of AARM and AMS foliations thus reveal shear-sense indicators with the younger AARM foliation lying furthest from the shear plane (Fig. 9). Our interpretation is essentially that small strains ($\gamma < 3$) rotated pre-existing fabrics produced initially by stress-controlled crystallization.

An alternative interpretation, more appropriate to large strains, is that rotation is primarily strain-influenced (Keith Benn, pers. commun., 1998). Due to the rigidity of the anorthosite and the low internal strain of its mafic silicates and ferromagnetic accessories this is not a major concern in this study. However, for more ductile rocks in the region where similar conclusions have been drawn the criticism warrants attention. Consider two extreme possible cases for grain rotation (Borradaile, 1993a) and the complexity they introduce, notwithstanding the assumption of perfect simple shear.

The first case, perfect rigid body rotation, excludes intergranular strain and requires that the marker grains align by rotating through a matrix of

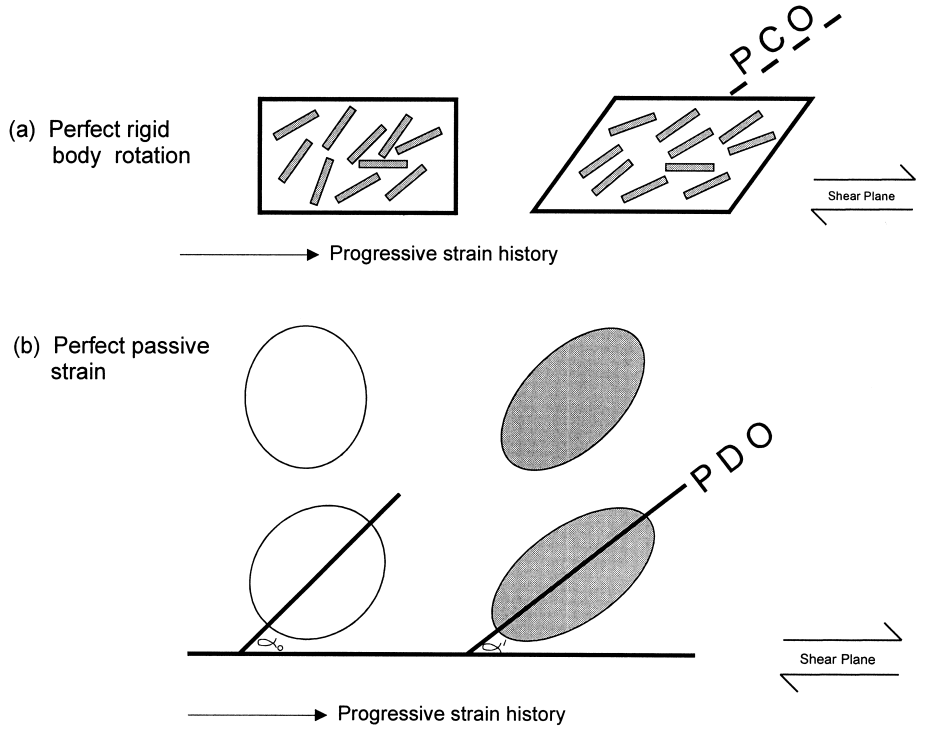

Fig. 10. Two idealized models of particle alignment by strain. *PCO* = preferred crystallographic orientation; *PDO* = preferred dimensional orientation.

negligible viscosity, avoiding mutual impingement (Fig. 10a). In two dimensions and for the case of simple shear (strain only in a plane perpendicular to the shear plane), the angle of grain long-axis to the shear plane is approximately given by:

$$\cot(\alpha') = \sqrt{\frac{A}{C}} \cdot \left[\tan(\gamma\sqrt{[A \cdot C]} + \arctan\left(\sqrt{\frac{C}{A}} \cdot \cot\alpha_0\right)\right] \quad (1)$$

in which α_0 = initial angle between long axis and shear plane, α' = final angle, γ = shear strain, R = grain aspect ratio (length/width) and

$$A = \frac{R^2}{R^2+1} \quad C = \frac{1}{R^2+1}$$

from Ghosh and Ramberg (1976). Therefore, even with the idealized conditions of perfectly rigid markers, zero viscosity matrix, $Y = 0$ and shear confined to two-dimensional strain, the rate of rotation depends on initial angle and aspect ratio. In our study this oversimplified model is the closest to the case of rotation of partially prealigned, rigid crystals to enhance and rotate a preferred *crystallographic* orientation (PCO, Fig. 10a).

An other extreme simplification, passive rotation, assumes that the grain is indistinguishable from the matrix in terms of physical properties, acting rather like a marker distinguished only by some nonmaterial feature such as colour. This applies readily to any object with an envelope that appears to be approximately elliptical, e.g., clastic grains, pebbles, concretions, lava pillows (Borradaile, 1987b). Rotation is apparent rather than real because the outline behaves like a rubber band lying on a flat surface that is pulled in a direction different from its long axis. This is clearly demonstrated by the upper elliptical marker in Fig. 10b. It has such a low aspect ratio that its rotation would be negligible if it responded rigidly. Here, however, the perfectly 'ductile' response can pull the ellipse out toward the long axis of the finite strain ellipse producing an apparently large rotation. Such an alignment affects shape directly and is more

properly called a preferred *dimensional* orientation (PDO, Fig. 10b). For a general strain history, including perfect simple shear, the equation relating the initial and finite particle orientations *with respect to the long axis of the strain ellipse* (rather than the shear plane) is:

$$\tan 2\phi = \frac{2\sqrt{R_s}\cdot(R_0-1)\cdot\sin 2\theta}{(R_0+1)\cdot(R_s-1)+(R_0-1)\cdot(R_s+1)\cdot\cos 2\theta} \quad (2)$$

where $\sqrt{R_0}$ = initial aspect ratio, $\sqrt{R_f}$ = final aspect ratio, $\sqrt{R_s}$ = strain ratio, θ = initial angle between long axis and finite strain ellipse long axis, ϕ = final angle (Ramsay, 1967, eqs. 5–22). This is considerably more complex than the more commonly considered passive *line* rotation:

$$\cot\alpha' = \gamma + \cot\alpha_0 \quad (3)$$

where γ = shear strain, α_0 = the initial angle with the shear plane and α' = the final angle (Ramsay, 1967, eqs. 3–7). Nevertheless, where grain aspect ratio is not very large (<10), it is advisable to consider the rotation being controlled by reshaping mechanism described graphically above and by Eq. 2. Simple shear of passive objects produces a slower alignment than of passive linear markers (Fig. 11).

Thus, if finite strain causes the grain alignment, the final orientations of two mineral foliations depend on grain aspect ratio, initial orientation, the relative roles of rigid/passive rotation and the relative ages of the two foliations in the strain history. Moreover, grain shape and initial orientation are not unique; their frequency distributions also affect the outcome (Borradaile, 1987b). The author can provide a shareware computer program to simulate these effects and perform a variety of strain analysis techniques (RfPhi.EXE obtainable from Borradaile@LakeheadU.CA).

Clearly, if finite strain were the dominating control on the fabric orientations and if the shear strain were sufficiently large ($\gamma > 3$), one could expect a variety of outcomes, in which either AARM or AMS foliations could have rotated closer to the shear plane, depending on the numerous variables (Eqs. 1 and 3). For example, if the mica subfabric turned more slowly toward the shear plane than more equidimensional grains such as magnetite, AMS foliation would be further from the shear plane than the AARM foliation, contradicting our results and those of earlier studies. Such concerns are limited to materials with suitable aspect ratios and large strains, e.g., magmatic flow (Benn and Allard (1989), high temperature deformation (Blumenfeld and Bouchez, 1988) or soft-sediment deformation.

We conclude that the noncoaxial strain history with moderate regional dextral shear on an E–W vertical shear plane progressively produced and aligned S_1, AMS and AARM foliations with the shear plane. Near Bad Vermilion Lake this reveals dextral shear (Fig. 8b). For the Rainy Lake block, the angular relationships of foliations similarly reveal north-side-up displacement (Fig. 8a).

Feldspars show no clear preferred orientation so that it is unlikely that AMS is influenced by their sparse ferromagnetic inclusions, whose orientations could be controlled by host crystallography. A previous rock-magnetic study of ferromagnetic inclusions in silicates shows that even where silicates posses significant ferromagnetic inclusions their intracrys-

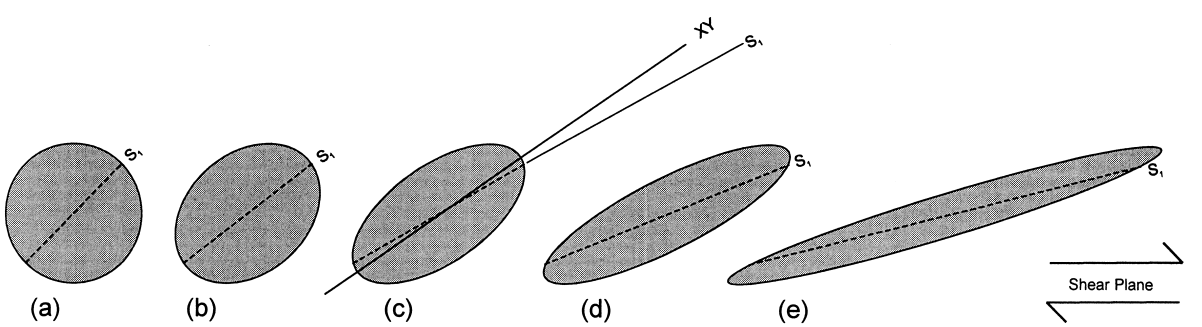

Fig. 11. In homogeneous strain with a progressive noncoaxial history like simple shear, a passive linear marker will spin more rapidly toward the shear plane than a marker defined by some closed loop.

talline angular dispersion combined with the scattered orientation distribution of host grains results in negligible whole-rock magnetic anisotropy (Borradaile, 1994). Indeed, if this were not so, palaeomagnetic work would scarcely be possible in igneous rocks. For this reason, and from basic petrographic observations and the normal progression of metamorphic reactions we argue that the intergranular ferromagnetic grains grew late. We attribute their well developed, consistent AMS to stress-controlled crystallization. In contrast, S_1 is a rough, poorly, locally developed fabric of weakly deformed feldspar that could not account for such a consistent AMS. AMS foliation, due mainly to mafic silicates, is offset anticlockwise in plan view from S_1. Since the samples represent homogeneously strained portions of the rock, large-scale E–W dextral shear can account for the AMS foliation of biotite and chlorite that grew late in the metamorphic sequence. On the other hand, S_1 represents a longer history, recorded by feebly developed feldspar fabrics. AARM foliation might be slightly offset counterclockwise from S_1, contradicting our model (Fig. 9), but in individual subareas where there are sufficient data to corroborate our shear-sense interpretations regionally. Because AARM foliation is the youngest it may reveal a late component in the noncoaxial strain history. If the plan-view counterclockwise interpretation is correct, this may represent E–W sinistral shear.

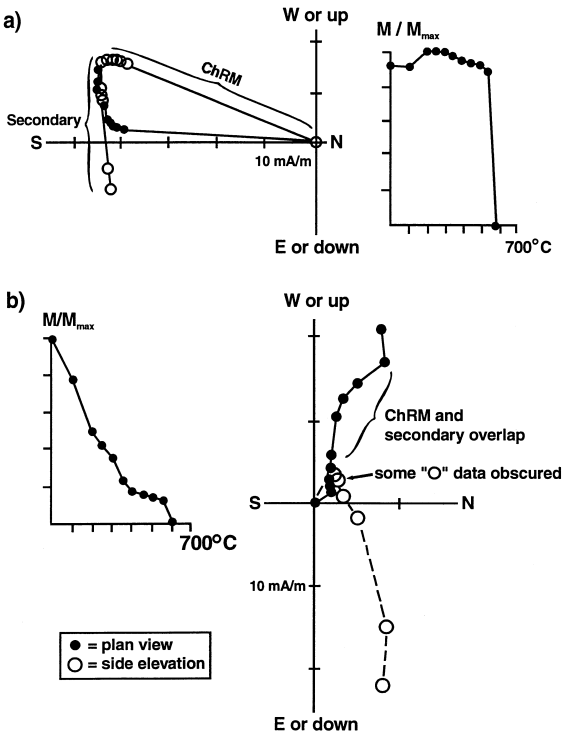

Fig. 12. Typical vector plots (Zijderveld, 1967) for the remanences in the anorthosites. (a) Most samples show two magnetization components; a young one down to the north, that may be VRM in the present geomagnetic field. However, they also show a strong, variably oriented characteristic component due to effects of deformation. (b) Some samples show two curved demagnetization trajectories. Although normally considered due to overlapping blocking temperature spectra, it could also be due to slowly acquired remanence accompanying tilting.

5. The palaeomagnetic record

Incremental thermal demagnetization was successful for 42 samples over a temperature range up to 700ºC. Normally, at least eleven demagnetization steps were made. We analyzed demagnetization trajectories on the vector plots by principal component analysis (Kirschvink, 1980). This was done interactively during the experiments using a combined spinner–magnetometer control and data interpretation program. Most samples demagnetized completely, just below 600ºC (e.g., intensity graphs inset in Fig. 12). This suggests that magnetite carries the remanence, rather than the pyrrhotite whose Curie point is around 300ºC.

In most samples, steep northwards, downwards secondary components unblock between 200ºC and 300ºC (Figs. 12 and 13c, d). They have a Fisher mean orientation of 004/67, close to the present geomagnetic field. They could represent a modern viscous overprint because it is not deflected systematically in respect to structural position in the area. However, numerous posttectonic or late syntectonic intrusions about 100 km to the east have similar remanence directions that were shown to be primary (Dunlop, 1979a, 1983, 1984a,b, 1985). By comparison, our secondary component could be a posttectonic, late Archaean remanence that is fortuitously close to the present geomagnetic field direction.

The characteristic remanence that we consider to be primary has a bimodal distribution at 293/46 and 084/-63 (Fig. 13a, b). Although these are not quite

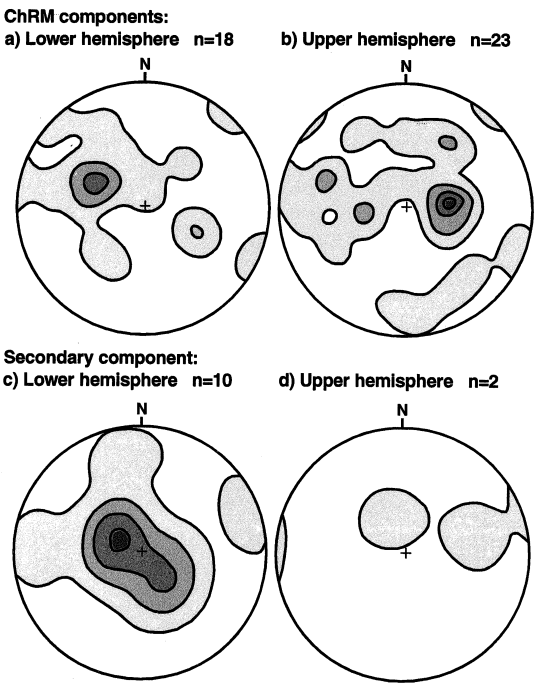

Fig. 13. Characteristic components of remanence cluster on the upper and lower hemisphere but they are not antipodal. They may represent a Normal/Reverse pair distorted by the regional shortening. This is possible because NW–SE regional shortening is which could steepen both the (a) down-maximum and (b) up-maximum to their present angular relationship. Clear secondary components (c, d) are generally downward and north.

antiparallel, they could represent a normal and reversed polarity pair, bearing in mind the effects of deformation and the unknown intervals of geomagnetic reversals in the Archaean. The 41 characteristic remanences recognized by principal component analysis show a weak NW–SE girdle (Fig. 13a, b), approximately perpendicular to the anorthosite sills. Down-seeking and up-seeking maxima lie in a girdle parallel to the regional horizontal shortening direction. This could explain the two maxima as a Normal/Reverse pair steepened toward a vertical orientation so that they are no longer antiparallel. It is now well accepted that stable remanence directions may rotate under the influence of small shortening strains, e.g., ~30%, associated with the initiation of cleavage in sediments elsewhere (McLelland-Brown, 1982; Facer, 1983; Schwartz and van der Voo, 1984; Hirt et al., 1986; Lowrie et al., 1986; van der Pluijm, 1987; Cogné and Perroud, 1987; Henry, 1992; Borradaile, 1993b, 1997). Here, strain shadows reveal shortening of $\leq$20% so that we could expect a modest dispersion of stable remanence vectors.

For some samples, the vector plots showed a curved trajectory representing some combination of differently oriented characteristic sub-components (e.g., Fig. 12b). Normally, one interprets this as overlapping blocking temperature spectra of multiple components *of similar age* (Dunlop, 1979b; Hoffman and Day, 1978; Halls, 1979; Dunlop and Özdemir, 1997). However, it seems too much of a coincidence that the vector-trajectory curves lie in NW–SE vertical planes, parallel to the NW–SE regional shortening direction.

We envision that as the anorthosite tilted to a steeper angle, earlier magnetic components were rotated with it and younger components were imposed initially at gentler angles to the sill, only to be rotated southward subsequently (Fig. 15). The progressive southward rotation eventually permitted the acquisition of softer, younger components almost parallel to the sills. This sequence accounts for the range of principal components that we find and for their unblocking temperatures. Syntectonic magnetization and remagnetization is documented from other studies and regions (e.g., Kligfield et al., 1983; Miller and Kent, 1986; Kodama, 1988; Vetter et al.,

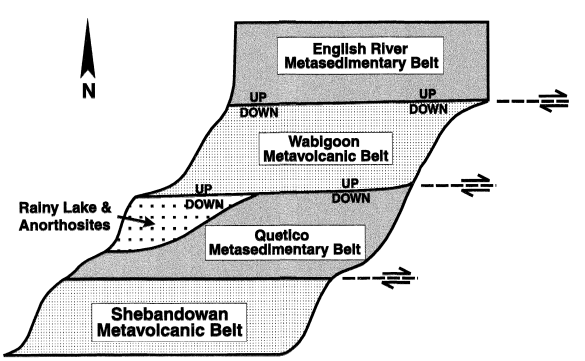

Fig. 14. Schematic map shows the sense of terrain-boundary shear and the senses of vertical motion on the boundaries. Magnetic fabrics confirm this kinematic pattern for the eastern part of the Shebandowan Belt (Borradaile and Spark, 1991; Borradaile and Dehls, 1993) and for the southern margin of the English River Belt (Borradaile et al., 1993a,b). Structural mapping supports dextral transpression of the margins of the Quetico Belt elsewhere (Hudleston, 1976; Borradaile, 1988; Hudleston et al., 1988).

1989; Hudson et al., 1989; Stamatakos and Kodama, 1991a,b; Borradaile, 1997). It may not be necessary to invoke conveniently syntectonic thermal or chemical events to produce the required magnetizations. Experiments suggest that pulses of stress may trigger remagnetization in magnetite (Borradaile, 1996).

6. Discussion

S_1 fabric developed first in these rocks, expressing itself permanently in feldspars, as a cataclastic foliation. Within the anorthosite, a single deformation phase produced an integral schistosity-lineation fabric with dominant foliation (S>L). This is barely discernible in some parts of the massive, coarse-grained anorthosite. The growth of biotite, chlorite and other mafic minerals contributed to the predominantly planar AMS fabric, sometime after the initiation of S_1. The plan-view angular offset between the AMS foliation and S_1 is compatible with dextral shear along a vertical SW–NE Seine River Fault in the eastern part of the intrusion, south of Bad Vermilion Lake (Fig. 15). For the main part of the intrusions, near Rainy Lake, the magnetic fabric geometry also favours north-side-up shear. Comparisons of AMS and still younger AARM foliation orientations suggest that this shear sense may have persisted later in the deformation history, at least in some subareas. Localized E–W sinistral shear near Bad Vermilion Lake is a local strain heterogeneity modifying the more important and regionally significant north-side-up shear on the north side of the Quetico subprovince (Figs. 14 and 15). We con-

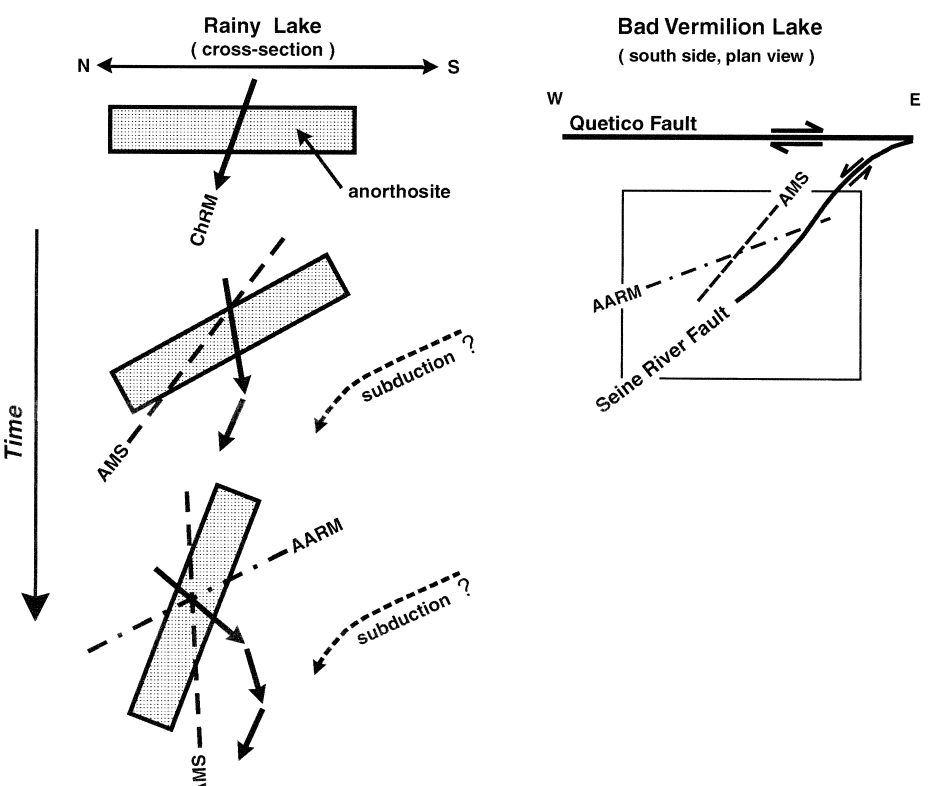

Fig. 15. Schematic local cross-section for Rainy Lake and map for Bad Vermillion area. The Rainy Lake *section* reveals progressive tilting of the anorthosites from the progressive magnetizations (ChRM = characteristic remanent magnetization). The successive development of AMS (silicates), then AARM (magnetite) confirm the progressive south-side-down movement. Together with tilting of the anorthosite this confirms suggestions by other authors that subduction was to the north. The Bad Vermilion area shows a local complexity because the anorthosite occurs in a strain shadow against a conjugate fault (Borradaile and Dehls, 1993). Thus locally, on the south side of this block, the shear sense is sinistral. However, AMS foliation is still younger than AARM foliation.

sider that the north-side-up shear over the bulk of the Rainy Lake anorthosite and northwards steepening of the anorthosite sills (Figs. 12 and 15) accompanied northwards subduction with dextral transpression of terrain boundaries (Fig. 14). This much agrees with the S_1, AMS foliation and AARM foliation kinematics and is compatible with the dextral transpression inferred by structural studies (Hudleston et al., 1988; Borradaile et al., 1988).

Characteristic magnetizations unblock >300ºC and disperse in a NW–SE girdle with two, not quite antiparallel maxima. The girdle contains the NW–SE horizontal regional shortening direction. Moreover, S_1–AMS–AARM kinematics favour this as the plane containing poles to tilted surfaces during progressive steepening. Therefore, the two primary remanence maxima could have been originally antiparallel, their present steeper attitudes due to NW–SE shortening or compression. In that case, at least one geomagnetic reversal could have occurred in this interval. Further evidence for the close timing of characteristic magnetization and tectonism comes from vector plots that show 'smeared' or curving paths. It is reasonable to assume that the now vertical anorthosite sheet was initially gently dipping. Thus, the simplest interpretation is that the anorthosite tilted to acquire successive components of magnetization in the geomagnetic field at successively gentler angles to the sheet. Palaeomagnetic evidence therefore supports the geological contention that the anorthosite tilted progressively northward (Fig. 15).

Acknowledgements

This work was supported by operating and research equipment grants to G. Borradaile from the Natural Sciences and Engineering Research Council of Canada. Keith Benn and Ben van der Pluijm provided constructive and perceptive reviews.

References

Bauer, R.L., Hudleston, P.J., Southwick, D.L., 1992. Deformation across the western Quetico subprovince and adjacent boundary regions in Minnesota. Can. J. Earth Sci. 29, 2087–2103.

Benn, K., Allard, B., 1989. Preferred mineral orientations related to magmatic flow in ophiolite layered gabbros. J. Petrol. 30, 925–946.

Blumenfeld, P., Bouchez, J.-L., 1988. Shear criteria in granite and migmatite deformed in the magmatic and solid states. J. Struct. Geol. 10, 361–372.

Borradaile, G.J., 1987a. Anisotropy of magnetic susceptibility: rock composition versus strain. Tectonophysics 138, 327–329.

Borradaile, G.J., 1987b. Analysis of strained sedimentary fabrics: review and tests. Can. J. Earth Sci. 24, 442–455.

Borradaile, G.J., 1988. Magnetic susceptibility, petrofabrics and strain. Tectonophysics 156, 1–20.

Borradaile, G.J., 1991. Correlation of strain with anisotropy of magnetic susceptibility (AMS). Pure Appl. Geophys. 135, 15–29.

Borradaile, G.J., 1993a. The rotation of magnetic grains. Tectonophysics 221, 381–384.

Borradaile, G.J., 1993b. Strain and magnetic remanence. J. Struct. Geol. 15, 383–390.

Borradaile, G.J., 1994. Paleomagnetism carried by crystal inclusions: the effect of preferred crystallographic orientations. Earth Planet. Sci. Lett. 126, 171–182.

Borradaile, G.J., 1996. Experimental stress remagnetization of magnetite. Tectonophysics 261, 229–248.

Borradaile, G.J., 1997. Deformation and paleomagnetism. Geophys. Surv. 18, 405–435.

Borradaile, G.J., Dehls, J.F., 1993. Regional kinematics inferred from magnetic subfabrics in Archean rocks of northern Ontario. Can. J. Struct. Geol. 15, 383–390.

Borradaile, G.J., Henry, B., 1997. Tectonic applications of magnetic susceptibility and its anisotropy. Earth Sci. Rev. 42, 49–93.

Borradaile, G.J., Spark, R.N., 1991. Deformation of the Archean Quetico–Shebandowan subprovince boundary in the Canadian Shield near Kashabowie, northern Ontario. Can. J. Earth Sci. 28, 116–125.

Borradaile, G.J., Stupavsky, M., 1995. Anisotropy of magnetic susceptibility: measurement schemes. Geophys. Res. Lett. 15, 1957–1960.

Borradaile, G.I., MacKenzie, A., Jensen, E., 1990. Silicate versus trace mineral susceptibility in metamorphic rocks. J. Geophys. Res. 95, 8447–8451.

Borradaile, G.J., Bayly, M.B., Powell, C.McA., 1982. Atlas of Deformational and Metamorphic Rock Fabrics. Springer, Berlin, 551 pp.

Borradaile, G., Sarvas, P., Dutka, R., Stewart, R., Stubley, M., 1988. Transpression in slates along the margin of an Archean gneiss belt, northern Ontario — magnetic fabrics and petrofabrics. Can. J. Earth Sci. 25, 1069–1077.

Borradaile, G.I., Werner, T., 1994. Magnetic anisotropy of some phyllosilicates. Tectonophysics 235, 233–248.

Borradaile, G.J., Werner, T., Dehls, J.F., Spark, R.N., 1993a. Archean regional transpression and paleomagnetism in northwestern Ontario, Canada. Tectonophysics 220, 117–125.

Borradaile, G.J., Stewart, R.A., Werner, T., 1993b. Uplift of an Archean subprovince boundary from magnetic fabrics. Tectonophysics 227, 1–15.

Cogné, J.-P., Perroud, H., 1987. Unstraining paleomagnetic vectors: the current state of debate. Eos 68, 705–712.

Dunlop, D.J., 1979a. A regional paleomagnetic study of Archean rocks from the Superior Geotraverse area, northwestern Ontario. Can. J. Earth Sci. 16, 1909–1919.

Dunlop, D.J., 1979b. On the use of Zijderveld vector diagrams in multicomponent paleomagnetic studies. Phys. Earth Planet. Inter. 20, 12–24.

Dunlop, D.J., 1983. Paleomagnetism of Archean rocks from northwestern Ontario: Wabigoon gabbro, Wabigoon Subprovince. Can. J. Earth Sci. 20, 1805–1817.

Dunlop, D.J., 1984a. Paleomagnetism of Archean rocks from northwestern Ontario, II. Shelley Lake granite, Quetico Subprovince. Can. J. Earth Sci. 21, 869–878.

Dunlop, D.J., 1984b. Paleomagnetism of Archean rocks from northwestern Ontario, IV. Burchell Lake granite, Wawa–Shebandowan Subprovince. Can. J. Earth Sci. 21, 1098–1104.

Dunlop, D.J., 1985. Paleomagnetism of Archean rocks from northwestern Ontario, V. Poohbah Lake alkaline complex, Quetico Subprovince. Can. J. Earth Sci. 22, 27–38.

Dunlop, D.J., Özdemir, Ö., 1997. Rock Magnetism: Fundamentals and Frontiers. Cambridge Studies in Magnetism, Cambridge University Press, Cambridge, 573 pp.

Facer, R.A., 1983. Folding, strain, and Graham's fold test in paleomagnetic investigations. Geophys. J. R. Astron. Soc. 72, 165–171.

Ghosh, S.K., Ramberg, H., 1976. Reorientation of inclusions by combination of pure shear and simple shear. Tectonophysics 34, 1–70.

Halls, H.C., 1979. Separation of multicomponent NRM: combined use of difference an resultant magnetization vectors. Earth Planet. Sci. Lett. 43, 303–308.

Henry, B., 1989. Magnetic fabric and the orientation tensor of minerals in rocks. Tectonophysics 165, 21–27.

Henry, B., 1990. Magnetic fabric implications for the relationships between deformation mode and grain growth in slates from the Borrowdale Volcanic Group in the English Lake District. Tectonophysics 178, 225–230.

Henry, B., 1992. Structural implications of paleomagnetic data from Pelvoux–Belledonne area (French Alps). Tectonophysics 216, 327–338.

Hirt, A.M., Lowrie, W., Pfiffner, O.A., 1986. A paleomagnetic study of tectonically deformed red beds of the Lower Glarus Nappe Complex, Eastern Switzerland. Tectonics 5, 723–731.

Hoffman, K.A., Day, R., 1978. Separation of multi-component NRM: a general method. Earth Planet. Sci. Lett. 40, 433–438.

Housen, B.A., van der Pluijm, B.A., 1990. Chlorite control of correlations between strain and anisotropy of magnetic susceptibility. Phys. Earth Planet. Inter. 61, 315–323.

Hudleston, P.J., 1976. Early deformational history of Archean rocks in the Vermilion district, northeastern Minnesota. Can. J. Earth Sci. 13, 579–592.

Hudleston, P.J., Schultz-Ela, D., Southwick, D.L., 1988. Transpression in an Archean greenstone belt, northern Minnesota. Can. J. Earth Sci. 25, 1060–1068.

Hudson, M.R., Reynolds, R.L., Fishman, N.S., 1989. Synfolding magnetization on the Jurassic Preuss sandstone, Wyoming–Idaho–Utah thrust belt. J. Geophys. Res. 94B, 13681–13705.

Jackson, M., 1991. Anisotropy of magnetic remanence: a brief review of mineralogical sources, physical origins, and geological applications and comparison with susceptibility anisotropy. Pure Appl. Geophys. 136, 1–28.

Jackson, M., Tauxe, L., 1991. Anisotropy of magnetic susceptibility and remanence: developments in the characterization of tectonic, sedimentary and igneous fabric. US National Report to International Union of Geodesy and Geophysics, Rev. Geophysics Supplement, pp. 371–376.

Jelinek, V., 1981. Characterization of the magnetic fabrics of rocks. Tectonophysics 79, T63–T67.

Kirschvink, J.L., 1980. The least-square line and plane and the analysis of palaeomagnetic data. Geophys. J. R. Astron. Soc. 62, 699–718.

Kligfield, R., Lowrie, W., Hirt, A., Siddans, A.W.B., 1983. Effect of progressive deformation on remanent magnetization of Permian Redbeds from the Alpes Maritimes (France). Tectonophysics 97, 59–85.

Kodama, K.P., 1988. Remanence rotation due to rock strain and the stepwise application of the fold test. J. Geophys. Res. 93, 3357–3371.

Lowrie, W., Hirt, A.M., Kligfield, R., 1986. Effects of tectonic deformation on the remanent magnetization of rocks. Tectonics 5, 713–722.

McCabe, C., Jackson, M., Ellwood, B., 1985. Magnetic anisotropy in the Trenton Limestone: results of a new technique, anisotropy of anhysteretic susceptibility. Geophys. Res. Lett. 12, 333–336.

McLelland-Brown, E., 1982. Paleomagnetic studies of fold development and propagation in the Pembrokeshire Old Red Sandstone. Tectonophysics 98, 131–149.

Miller, J.D., Kent, D.V., 1986. Synfolding and prefolding magnetizations in the Upper Devonian Catskill Formation of Eastern Pennsylvania: implications for the tectonic history of Acadia. J. Geophys. Res. 91, 12791–12803.

Percival, J.A., 1989. A regional perspective of the Quetico metasedimentary belt, Superior Province, Canada. Can. J. Earth Sci. 26, 677–693.

Ramberg, H., 1975. Particle paths, displacement and progressive strain applicable to rocks. Tectonophysics 28, 1–37.

Ramsay, J.G., 1967. Folding and Fracturing of Rocks. McGraw-Hill, New York, NY, 578 pp.

Rochette, P., Jackson, M.J., Aubourg, C., 1992. Rock magnetism and the interpretation of anisotropy of magnetic susceptibility. Rev. Geophys. 30, 209–226.

Sawyer, E.W., 1983. The structural history of a part of the Archean Quetico metasedimentary belt, Superior Province, Canada. Precambrian Res. 22, 271–294.

Schwartz, S.Y., van der Voo, R., 1984. Paleomagnetic study of thrust sheet rotation during foreland impingement in the Wyoming–Idaho overthrust belt'. J. Geophys. Res. 89, 10077–10086.

Stamatakos, J., Kodama, K.P., 1991b. The effects of grain-scale deformation on the Bloomsburg formation pole. J. Geophys. Res. 96, 17919–17933.

Stamatakos, J., Kodama, K.P., 1991a. Flexural flow folding and the paleomagnetic fold test: an example of strain reorientation of remanence in the Mauch Chunk Formation. Tectonics 10, 807–819.

Stephenson, A., Sadikun, S., Potter, D.K., 1986. A theoretical and experimental comparison of the anisotropies of magnetic susceptibility and remanence in rocks and minerals. Geophys. J. R. Astron. Soc. 84, 185–200.

Van der Pluijm, B.A., 1987. Grain scale deformation and the fold test — evaluation of synfolding remagnetization. Geophys. Res. Lett. 14, 155–157.

Vetter, J.R., Kodama, K.P., Goldstein, A., 1989. Reorientation of remanent magnetism during tectonic fabric development: an example from the Waynesboro Formation, Pennsylvania, USA. Tectonophysics 165, 29–39.

Werner, T., 1997. Experimental designs for determination of the anisotropy of remanence-test of the efficiency of least-square and bootstrap methods applied to metamorphic rocks from southern Poland. Phys. Chem. Earth 22, 131–136.

Werner, T., Borradaile, G.J., 1996. Paleoremanence dispersal across a transpressed Archean terrain: Deflection by anisotropy or by late compression? J. Geophys. Res. 101, 5531–5545.

Williams, H.R., Stott, G.M., Thurston, P.C., Sutcliffe, R.H., Bennett, G., Easton, R.M., Armstrong, D.K., 1992. Tectonic evolution of Ontario: summary and synthesis. In: The Geology of Ontario. Ontario Geological Survey, Spec. Vol. 4, part 2, pp. 1255–1334.

Zijderveld, J.D.A., 1967. A.C. demagnetization of rocks: Analysis of results. In: Collinson, D.W., Creer, K.M., Runcorn, S.K. (Eds.), Methods in Paleomagnetism. Elsevier, New York, pp. 254–256.